

# Kapundaite, $(\text{Na,Ca})_2\text{Fe}_4^{3+}(\text{PO}_4)_4(\text{OH})_3 \cdot 5\text{H}_2\text{O}$ , a new phosphate species from Toms quarry, South Australia: Description and structural relationship to mélonjosephite

STUART J. MILLS,<sup>1,2,\*</sup> WILLIAM D. BIRCH,<sup>2</sup> ANTHONY R. KAMPF,<sup>3</sup> ANDREW G. CHRISTY,<sup>4</sup>  
JOSEPH J. PLUTH,<sup>5</sup> ALLAN PRING,<sup>6</sup> MATI RAUDSEPP,<sup>1</sup> AND YU-SHENG CHEN<sup>7</sup>

<sup>1</sup>Department of Earth and Ocean Sciences, University of British Columbia, Vancouver, British Columbia V6T 1Z4, Canada

<sup>2</sup>Geosciences, Museum Victoria, GPO Box 666, Melbourne, Victoria 3001, Australia

<sup>3</sup>Mineral Sciences Department, Natural History Museum of Los Angeles County, 900 Exposition Boulevard, Los Angeles, California 90007, U.S.A.

<sup>4</sup>Research School of Earth Sciences, The Australian National University, Canberra, ACT 0200, Australia

<sup>5</sup>Department of Geophysical Sciences, Center for Advanced Radiation Sources and Materials, University of Chicago, 5734 S. Ellis Avenue, Chicago, Illinois 60637-1434, U.S.A.

<sup>6</sup>Mineralogy Department, South Australian Museum, North Terrace, Adelaide, South Australia 5000, Australia

<sup>7</sup>Center for Advanced Radiation Sources, University of Chicago, 5640 S. Ellis Avenue, Chicago, Illinois 60637-1434, U.S.A.

## ABSTRACT

Kapundaite, ideally  $(\text{Na,Ca})_2\text{Fe}_4^{3+}(\text{PO}_4)_4(\text{OH})_3 \cdot 5\text{H}_2\text{O}$ , is a new mineral (IMA2009-047) from Toms phosphate quarry, Kapunda, South Australia, Australia. The new mineral occurs as cavernous aggregates of fibers up to several centimeters across, associated with leucophosphite, natrodufenite, and meurigite-Na crystals and amorphous brown, black, and/or greenish coatings. Individual kapundaite crystals are very thin flattened fibers up to a few millimeters in length, but typically no more than a few micrometers in thickness. The main form observed is  $\{100\}$ ; other forms in the  $[010]$  zone are present, but cannot be measured. Crystals of kapundaite are pale to golden yellow, transparent to translucent, have a yellow streak and silky luster, and are non-fluorescent. Mohs hardness is estimated to be about 3; no twinning or cleavage was observed. Kapundaite is biaxial (+), with indices of refraction  $\alpha = 1.717(3)$ ,  $\beta = 1.737(3)$ , and  $\gamma = 1.790(3)$ .  $2V$  could not be measured;  $2V_{\text{calc}}$  is  $64.7^\circ$ . The optical orientation is  $Z = \mathbf{b}$ ,  $Y \approx \mathbf{c}$  with weak pleochroism:  $X =$  nearly colorless,  $Y =$  light brown,  $Z =$  pale brown; absorption:  $Y > Z > X$ . No dispersion was observed. The empirical chemical formula (mean of seven electron microprobe analyses) calculated on the basis of 24 O is  $(\text{Ca}_{1.13}\text{Na}_{0.95})_{22.08}(\text{Fe}_{3.83}^{3+}\text{Mn}_{0.03}\text{Al}_{0.02}\text{Mg}_{0.01})_{\Sigma 3.89}\text{P}_{3.92}\text{O}_{16}(\text{OH})_3 \cdot 5\text{H}_{2.11}\text{O}$ . Kapundaite is triclinic, space group  $P\bar{1}$ ,  $a = 6.317(5)$ ,  $b = 7.698(6)$ ,  $c = 9.768(7)$  Å,  $\alpha = 105.53(1)^\circ$ ,  $\beta = 99.24(2)^\circ$ ,  $\gamma = 90.09(2)^\circ$ ,  $V = 451.2(6)$  Å<sup>3</sup>, and  $Z = 1$ . The five strongest lines in the powder X-ray diffraction pattern are [ $d_{\text{obs}}$  in Å ( $hkl$ ): 9.338 (100) (001), 2.753 (64) ( $2\bar{1}1$ ), 5.173 (52) (011), 2.417 (48) ( $2\bar{1}3$ , 202,  $0\bar{1}4$ ), and 3.828 (45) ( $0\bar{2}1$ ). The crystal structure was solved from single-crystal X-ray diffraction data using synchrotron radiation and refined to  $R_1 = 0.1382$  on the basis of 816 unique reflections with  $F_o > 4\sigma F$ . The structure of kapundaite is based on a unique corrugated octahedral-tetrahedral sheet, which is composed of two types of chains parallel to  $\mathbf{a}$ . Kapundaite is structurally related to mélonjosephite. The mineral is named for the nearest town to the quarry.

**Keywords:** Kapundaite, new mineral, phosphate, Toms phosphate quarry, crystal structure, octahedral-tetrahedral sheet, mélonjosephite

## INTRODUCTION

Specimens of kapundaite were first collected in the mid-1980s by Vince Peisley (who has been the most dedicated mineral collector at the site and after whom peisleyite is named) at Toms phosphate quarry, Kapunda, South Australia ( $34^\circ 21'S$ ,  $138^\circ 55'E$ ), but were not thoroughly investigated at the time. Initial investigations suggested the mineral to be similar to meurigite (Birch et al. 1996; Kampf et al. 2007, 2009); however, several striking differences indicated it to be a distinct (and new) phase. In March 2009, Peisley discovered a more significant quantity of

the mineral, which has enabled its full characterization as a new species. The mineral data and name were approved by the IMA Commission on New Minerals, Nomenclature and Classification in September 2009 (IMA 2009-047). The name is for the closest town to the quarry, Kapunda, which is in turn derived from the Australian Aboriginal word “*cappie oonda*,” which applied to a spring near the present town site. Because no single specimen provided all of the data for the description, no specimen qualifies as the holotype, however, one co-type specimen is housed in the collections of Mineral Sciences Department, Natural History Museum of Los Angeles County (California, U.S.A.), catalog number 62495, and one in the collections of Museum Victoria (Melbourne, Australia), registration number M51138.

\* E-mail: smills@eos.ubc.ca

## OCCURRENCE AND GEOLOGY

Low-grade phosphorite horizons are widespread in the Cambrian marine sediments of the Kanmantoo Trough, in South Australia (Drexel and Preiss 1995). The phosphorites have been variably modified by metamorphism, followed by weathering and secondary enrichment during the Tertiary. As well as being a source of rock phosphate, recovered by intermittent mining since the early 1900s (Jack 1919; Johns 1962), the deposits contain a diverse range of phosphate minerals (Segnit and Watts 1981; Mills 2003; Mills et al. 2006), including new species. Several small quarries in the Angaston-Kapunda district, about 70 km northeast of Adelaide, are the type localities for peisleyite (Pilkington et al. 1982), aldermanite (Harrowfield et al. 1981), and angastonite (Mills et al. 2008). Toms quarry is situated about 8 km ESE of the town of Kapunda, and although it has only operated sporadically since the 1950s, remaining dumps have provided mineral collectors with a rich source of specimens containing such species as cacoxenite, childrenite, crandallite, fluellite, goethite, kingite, leucophosphite, minyulite, perhamite, variscite, wavellite (Mills 2003), meurigite-Na (Kampf et al. 2009), and peisleyite (Pilkington et al. 1982). The mineralization occurs in highly weathered, clay-rich, and ferruginous phosphorite, which unconformably overlies micaceous schists and marble (Jack 1919).

The original samples of kapundaite came from a goethite-rich exposure, which was at the time at floor level in the southeastern corner of the quarry. Now, following further working, the exposure is perched about 3 m above the quarry floor. In this zone, kapundaite occurs as linings to cavernous masses, which resemble open box-work replacements of massive phosphate mineralization, with dimensions on the scale of tens of centimeters. Several episodes of crystallization are evident, with compact fibrous aggregates commonly providing the substrate for later growth of more open arrays. In many specimens, the earlier generations of crystallization have been altered to an opaque fibrous pseudomorph. Kapundaite is closely associated with leucophosphite, natrodufrenite, and meurigite-Na on amorphous brown, black, or greenish coatings. The overall phosphate assemblage at Toms quarry has formed from the breakdown of fluorapatite in the presence of acidic Fe- and Al-bearing solutions. High localized concentrations of Na and K are reflected in the formation of the kapundaite-leucophosphite-natrodufrenite assemblage.

**FIGURE 1.** Kapundaite crystal ( $100 \times 9 \times 4 \mu\text{m}$ ) used in the optical and single-crystal studies (from NHMLAC specimen 62495).



## PHYSICAL AND OPTICAL PROPERTIES

Individual kapundaite crystals are very thin flattened fibers up to a few millimeters in length, but typically no more than a few micrometers in thickness (Fig. 1). The fibers occur in subparallel bundles, compact radial sprays, and feathery curving masses (Fig. 2). The

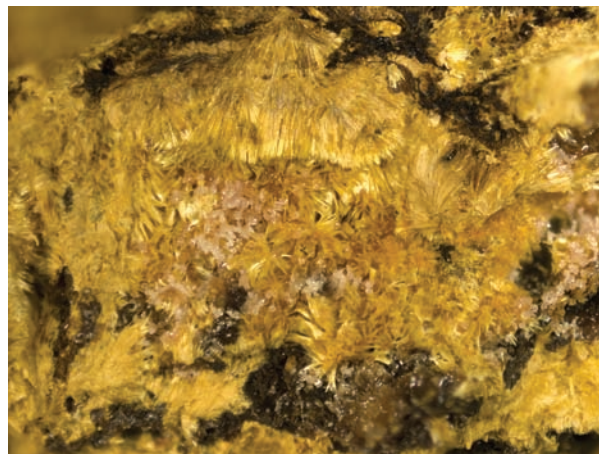


**FIGURE 2.** Kapundaite showing fibrous habit and distinctive golden yellow color. Field of view 5 mm across (NHMLAC specimen 62495).

fibers are flexible and have an irregular fracture. The main form observed is  $\{100\}$  (responsible for the tabular nature of the fibers) (Fig. 1); other forms in the  $[010]$  zone are present, but cannot be measured. Flattened terminations suggest that the form  $\{010\}$  is also present. Crystals of kapundaite are pale to golden yellow, transparent to translucent, have a yellow streak and silky luster, and are non-fluorescent. Mohs hardness is estimated to be about 3; no twinning or cleavage was observed. The density measured by the sink-float method in a mixture of diiodomethane and chloroform is  $2.93(3) \text{ g/cm}^3$ . The density calculated from the single-crystal unit cell and empirical formula is  $2.917 \text{ g/cm}^3$ .

Kapundaite is biaxial (+), with indices of refraction  $\alpha = 1.717(3)$ ,  $\beta = 1.737(3)$ , and  $\gamma = 1.790(3)$  measured in white light.  $2V$  could not be measured because of the unfavorable orientation of the fibers; the calculated  $2V$  is  $64.7^\circ$ . The optical orientation is  $Z = \mathbf{b}$ ,  $Y \approx \mathbf{c}$ ; kapundaite shows weak pleochroism:  $X =$  nearly colorless,  $Y =$  light brown,  $Z =$  pale brown; absorption:  $Y > Z > X$ . No dispersion was observed. The Gladstone-Dale compatibility  $[1 - (K_p/K_c)]$  (Mandarino 1981) is 0.012, indicating superior agreement between the chemistry, density, and average of the indices of refraction.

## CHEMICAL COMPOSITION

Quantitative wavelength-dispersive electron-microprobe analyses (7 points) were carried out on kapundaite using a Cameca SX 50 electron microprobe at the University of Melbourne. Operating conditions were 15 kV, with beam current of 20 nA and a  $5 \mu\text{m}$  beam diameter.  $\text{H}_2\text{O}$  was determined in duplicate using a Carlo Erba 1106 automatic CHN analyzer at the Microanalytical Unit in the Research School of Chemistry, Australian National University. The results, as well as the standards used, are shown in Table 1. Like many finely fibrous hydrated phases, kapundaite is a difficult mineral to analyze. To improve the analyses, a fragment from a compact aggregate was mounted in epoxy and polished, and moved slowly under the beam during the analysis to minimize volatile loss and surface damage. Despite the analytical total being slightly low, the analyses are consistent, show low standard deviations, and

yield a formula with satisfactory stoichiometry.

The mean composition of kapundaite corresponds to the empirical formula (calculated on the basis of 24 O apfu):  $(\text{Ca}_{1.13}\text{Na}_{0.95})_{\Sigma 2.08}(\text{Fe}_{3.83}\text{Mn}_{0.03}\text{Al}_{0.02}\text{Mg}_{0.01})_{\Sigma 3.89}\text{P}_{3.92}\text{O}_{16}(\text{OH})_3 \cdot 5\text{H}_2\text{O}$ . The simplified formula considering a 1:1 ratio of Na:Ca (the charged-balanced stoichiometry requires  $\text{Na} = \text{Ca} = 1$ ) is:  $(\text{Na,Ca})_2\text{Fe}_3^+(\text{PO}_4)_4(\text{OH})_3 \cdot 5\text{H}_2\text{O}$ , which

requires  $\text{Na}_2\text{O}$  3.84,  $\text{CaO}$  6.95,  $\text{Fe}_2\text{O}_3$  39.54,  $\text{P}_2\text{O}_5$  35.16,  $\text{H}_2\text{O}$  14.51 wt%, total 100 wt%.

## X-RAY DIFFRACTION

### Powder X-ray diffraction

X-ray powder-diffraction data were collected on Rigaku R-Axis Spider curved imaging plate microdiffractometer and monochromatized  $\text{MoK}\alpha$  radiation (Table 2). Unit-cell parameters refined from the powder data using Chekcell (Laugier and Bochu 2004) are  $a = 6.344(4)$ ,  $b = 7.728(5)$ ,  $c = 9.807(6)$  Å,  $\alpha = 105.526(6)$ ,  $\beta = 99.188(7)$ , and  $\gamma = 90.070(7)^\circ$ , which are in good agreement with those obtained from the single-crystal study (Table 3).

### Single-crystal X-ray diffraction

The structure data collection was performed at ChemMat-CARS, Sector 15, Advanced Photon Source at Argonne National Laboratory, U.S.A. A single crystal (used for the optical determinations) with the dimensions  $100 \times 9 \times 4$  μm was used for collection of intensity data (Table 3). The data set used in the refinement was collected using radiation from a water-cooled diamond (111) crystal at a wavelength of 0.41328 Å with higher harmonics removed using vertical Pt-coated Si mirrors and apertures to produce a  $200 \times 200$  m<sup>2</sup> beam. Data were recorded using an APEX II CCD (charge-coupled device) detector at fixed angle  $5^\circ 2\theta$  and scanning omega in  $0.5^\circ$  steps with 5 s counting per frame. The CCD detector was mounted on a Bruker diffractometer with a fixed  $\chi$  and with the  $\omega$  axis of the diffractometer in the plane of the ring. Data were integrated and corrected for Lorentz, polarization, and background effects using SAINTPLUS (Bruker 2003). Systematic errors, such as beam decay and absorption, were corrected with the program SADABS (Bruker 2003) on the basis of the intensities of equivalent reflections.

**TABLE 1.** Analytical data for kapundaite

Constituent	wt%	Range	Standard deviation	Probe standard
$\text{Na}_2\text{O}$	3.43	3.25–3.61	0.14	Albite
$\text{K}_2\text{O}$	0.01	0–0.02	0.01	Synthetic $\text{KTaO}_3$
$\text{CaO}$	7.40	7.14–7.51	0.15	Wollastonite
$\text{MgO}$	0.05	0.03–0.06	0.01	Periclase
$\text{MnO}$	0.25	0.18–0.29	0.04	Mn metal
$\text{Fe}_2\text{O}_3$	35.53	34.92–36.21	0.49	Hematite
$\text{Al}_2\text{O}_3$	0.11	0.07–0.15	0.04	Corundum
$\text{P}_2\text{O}_5$	32.35	31.56–33.30	0.56	Fluorapatite
$\text{H}_2\text{O}^*$	14.22	–	–	–
Total	93.35	92.25–95.18	1.16	–

\* Measured using the CHN method.

**TABLE 2.** X-ray powder diffraction data for kapundaite

<i>hkl</i>	<i>d</i> <sub>calc</sub>	<i>d</i> <sub>obs</sub>	<i>I</i> <sub>obs</sub>
001	9.034	9.338	100
010, 010	7.437	7.442	37
011	5.168	5.173	52
101	4.834	4.824	12
002	4.652	4.549	9
012	4.533		
021	3.828	3.828	45
012	3.537	3.536	27
022	3.385	3.389	26
$\bar{1}20, 120$	3.138	3.123	34
$200, 200$	3.124		
$201$	3.119	2.928	30
$\bar{2}11$	2.938		
$\bar{2}11$	2.928	2.817	33
$210, 210$	2.924		
201	2.825	2.753	64
202	2.815		
$211$	2.753	2.621	17
103	2.622	2.574	7
031	2.575	2.474	20
030, 030	2.479	2.417	48
$\bar{2}13$	2.419		
202	2.417	2.338	15
014	2.413		
$220, \bar{2}20$	2.344	2.259	2
$130, 130$	2.338		
221	2.334	2.116	26
033	2.257		
222	2.200	2.031	7
023	2.117		
$301$	2.107	1.983	10
$\bar{1}11$	2.037		
204	2.031	1.950	5
$302$	2.028		
$\bar{2}32$	1.989	1.929	7
$231$	1.989		
231	1.985	1.900	8
034	1.985		
$310, 310$	1.984	1.857	11
$230, 230$	1.983		
032	1.977	1.762	28
$\bar{1}34$	1.952		
$311$	1.947	1.856	multiple possible
015	1.932		
123	1.927	1.857	multiple possible
041	1.926		
multiple possible		1.900	8
040, 040	1.859	1.857	11
311	1.856	1.762	28
multiple possible		1.762	28

**TABLE 3.** Data collection and structure refinement details for kapundaite

Structural formula	$(\text{Na}_{1.34}\text{Ca}_{0.66})_{\Sigma 2}\text{Fe}_4(\text{PO}_4)_4(\text{OH})_3 \cdot 5\text{H}_2\text{O}$
Wavelength	0.41328 Å
Temperature	296(2) K
Space group	<i>P1</i>
Unit-cell dimensions	$a = 6.317(5)$ Å $b = 7.698(6)$ Å $c = 9.768(7)$ Å $\alpha = 105.53(1)^\circ$ $\beta = 99.24(2)^\circ$ $\gamma = 90.09(2)^\circ$
Z	1
Volume	451.2(6) Å <sup>3</sup>
Density (for formula above)	2.972 gm/cm <sup>3</sup>
Absorption coefficient	2.035 mm <sup>-1</sup>
<i>F</i> (000)	400
Crystal size	100 × 9 × 4 μm
θ range	1.26 to 18.95°
Index ranges	$-7 \leq h \leq 5$ , $-11 \leq k \leq 12$ , $-15 \leq l \leq 15$
Reflections collected/unique	5601/1513 [ $R_{\text{int}} = 0.0940$ ]
Reflections with $F_o > 4\sigma F$	816
Completeness to $\theta = 18.95^\circ$	39.2%
Refinement method	Full-matrix least-squares on $F^2$
Parameters refined	144
GoF	1.059
Final <i>R</i> indices [ $F_o > 4\sigma F$ ]	$R_1 = 0.1382$ , $wR_2 = 0.3288$
<i>R</i> indices (all data)	$R_1 = 0.2268$ , $wR_2 = 0.3868$
Largest diff. peak/hole	2.943 and $-1.371 e\text{-A}^{-3}$

Notes:  $R_{\text{int}} = \sum |F_o^2 - F_o^2(\text{mean})| / \sum F_o^2$ .  $\text{GoF} = S = \{ \sum [w(F_o^2 - F_c^2)]^2 / (n - p) \}^{1/2}$ .  $R_1 = \sum |F_o| - |F_c| / \sum |F_o|$ .  $wR_2 = \{ \sum [w(F_o^2 - F_c^2)]^2 / \sum [w(F_c^2)] \}^{1/2}$ .  $w = 1 / \{ \sigma^2(F_o^2) + (aP)^2 + bP \}$ ; where  $a = 0.1740$  and  $b = 24.8423$  and  $P = [2F_o^2 + \text{Max}(F_o, 0)] / 3$ .

The crystal structure of kapundaite was solved in  $P\bar{1}$  (space group no. 2) by direct methods using SHELXS-97 (Sheldrick 2008) and subsequent Fourier and difference Fourier syntheses, followed by anisotropic full-matrix least-squares refinements on  $F^2$  using SHELXL-97 (Sheldrick 2008). The final model converged to  $R_1 = 13.82\%$  for 816 reflections [ $F_o > 4\sigma F$ ] and 22.68% for all 1513 reflections. The nature of the crystal (small and thin), led to the high  $R$ -factor.

Although the Na/Ca site refined to 0.67 Na and 0.33 Ca, we regard the EMPA as a more reliable determinant of the relative amounts of Na and Ca present and have consequently assumed the Na/Ca site to be equally occupied by Na and Ca for the bond valence calculations. Bond valence calculations indicate that one O atom (designated OH) is a hydroxyl group and that three O atoms (designated OW1, OW2, and OW3) are water molecules; however, the quality of the data did not allow the determination of the H atom sites. Hydrogen bonds were assigned based upon O-O distances, reasonable bond geometries and bond valence considerations. No hydrogen bond acceptor is evident for the H atom of the OH group.

The refined atomic coordinates and displacement parameters are given in Table 4, polyhedral bond distances in Table 5, and a bond-valence analysis in Table 6.

#### DESCRIPTION OF THE STRUCTURE

The structure of kapundaite (Fig. 3) is based on a unique corrugated octahedral-tetrahedral sheet parallel to  $\{001\}$ . The Na/Ca site between the sheets is 8-coordinated, with three Na/Ca-O bonds to one sheet and one Na/Ca-O bond to the other sheet. The remaining four Na/Ca-O bonds are to  $H_2O$  molecules. Examination of the average bond distances for the  $FeO_6$  octahedra and the bond valence summations for the Fe sites clearly indicates that all Fe is 3+. The somewhat anomalous  $PO_4$  bond distances and the bond valence summations for the P sites are attributed more to the relatively low quality of the structure data, than to real structural anomalies.

The octahedral-tetrahedral sheet is composed of two types of chains parallel to the  $a$  direction. One chain consists of *trans*-edge-sharing octahedra decorated by  $PO_4$  tetrahedra linking free vertices of adjacent octahedra in a staggered arrangement (Fig. 4a). Topologically identical chains are found in the structures of

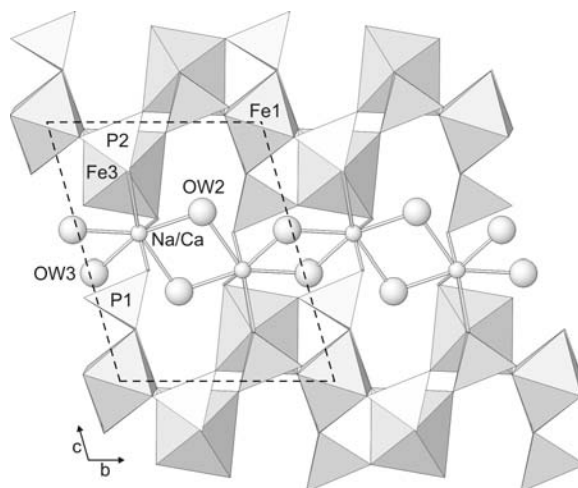


FIGURE 3. Structure of kapundaite viewed down  $a$ . Unit-cell outline in dashes.

TABLE 5. Selected bond distances (Å) in kapundaite

Na/Ca-O5	2.34(2)	Fe1-O4 (x2)	1.93(1)
Na/Ca-O2	2.42(3)	Fe1-O8 (x2)	2.04(2)
Na/Ca-OW2	2.45(2)	Fe1-OH (x2)	2.09(4)
Na/Ca-OW3	2.46(3)	<Fe1-O>	2.02
Na/Ca-OW3	2.46(3)		
Na/Ca-OW2	2.69(3)	Fe2-O3 (x2)	1.99(2)
Na/Ca-OW1	2.71(4)	Fe2-O8 (x2)	2.01(3)
Na/Ca-O6	2.77(3)	Fe2-OH (x2)	2.07(2)
<Na/Ca-O>	2.54	<Fe2-O>	2.02
P1-O1	1.52(2)	Fe3-O7	1.92(2)
P1-O2	1.54(2)	Fe3-O6	1.98(4)
P1-O3	1.58(3)	Fe3-OH	2.00(2)
P1-O4	1.64(4)	Fe3-O1	2.03(2)
<P1-O>	1.57	Fe3-O5	2.03(4)
		Fe3-OW1	2.20(1)
P2-O5	1.44(3)	<Fe3-O>	2.03
P2-O6	1.50(3)		
P2-O7	1.51(2)		
P2-O8	1.58(2)		
<P1-O>	1.51		
		<b>Hydrogen bonds</b>	
OW1-O2	2.57(5)	OW2-O4	2.72(3)
OW1'-O2	2.77(5)	OW2'-O3	2.81(4)
		OW3-O1	2.84(4)
		OW3'-O3	2.99(3)

Note: e.s.d. values given in parentheses.

TABLE 4. Atom coordinates and displacement parameters ( $\text{\AA}^2$ ) for kapundaite

	$x$	$y$	$z$	$U_{eq}$	$U_{11}$	$U_{22}$	$U_{33}$	$U_{23}$	$U_{13}$	$U_{12}$
Na/Ca	0.439(3)	0.7184(10)	0.4298(7)	0.056(10)	0.12(3)	0.016(4)	0.028(4)	0.008(3)	0.009(6)	0.004(8)
Fe1	0.5000	0.0000	0.0000	0.013(3)	0.02(1)	0.018(2)	0.004(1)	0.003(1)	0.002(2)	-0.009(4)
Fe2	0.0000	0.0000	0.0000	0.017(4)	0.03(1)	0.017(2)	0.003(1)	0.004(1)	0.002(2)	0.003(4)
Fe3	0.7976(12)	0.6972(5)	0.1730(3)	0.024(3)	0.02(1)	0.016(2)	0.033(2)	0.003(1)	0.010(2)	-0.003(3)
P1	0.177(2)	0.8785(8)	0.7118(6)	0.015(5)	0.01(1)	0.013(2)	0.026(2)	0.005(2)	0.009(3)	0.005(6)
P2	0.278(2)	0.6868(8)	0.1002(6)	0.021(5)	0.02(1)	0.012(2)	0.033(3)	0.010(2)	0.006(4)	0.002(5)
O1	0.832(5)	0.940(2)	0.323(2)	0.021(13)	0.02(4)	0.020(8)	0.024(6)	0.008(5)	-0.003(9)	-0.010(16)
O2	0.157(6)	0.723(2)	0.572(2)	0.023(15)	0.03(4)	0.015(7)	0.028(7)	-0.001(5)	0.014(10)	0.001(17)
O3	0.011(6)	0.143(2)	0.204(2)	0.034(17)	0.06(5)	0.019(8)	0.029(8)	0.007(6)	0.018(12)	0.002(18)
O4	0.414(6)	0.861(2)	0.802(2)	0.046(17)	0.09(5)	0.019(8)	0.026(7)	0.004(6)	-0.007(12)	-0.025(19)
O5	0.482(6)	0.686(2)	0.191(1)	0.019(3)						
O6	0.114(6)	0.683(2)	0.195(1)	0.020(3)						
O7	0.771(6)	0.463(2)	0.038(2)	0.024(3)						
O8	0.262(5)	0.871(2)	0.059(2)	0.017(13)	0.01(4)	0.018(8)	0.031(7)	0.012(6)	0.009(10)	0.002(16)
OH	0.242(6)	0.165(3)	0.976(2)	0.027(15)	0.03(4)	0.029(9)	0.027(7)	0.013(6)	-0.003(10)	-0.013(18)
OW1	0.831(6)	0.611(2)	0.372(2)	0.035(15)	0.07(5)	0.024(8)	0.023(7)	0.019(6)	0.007(11)	0.002(17)
OW2	0.351(8)	0.394(3)	0.349(2)	0.05(2)	0.08(6)	0.044(13)	0.036(9)	0.004(8)	0.005(14)	-0.02(3)
OW3	0.669(9)	0.979(3)	0.584(2)	0.06(2)	0.11(7)	0.011(7)	0.054(11)	0.013(7)	0.005(18)	0.02(2)

Notes: e.s.d. values given in parentheses. The occupancy of Na/Ca site refined to 0.67(7) Na and 0.33(7) Ca.

**TABLE 6.** Bond valence summations for kapundaite

	O1	O2	O3	O4	O5	O6	O7	O8	OH	OW1	OW2	OW3	$\Sigma_v$
Na/Ca		0.235			0.291	0.091				0.107	0.216	0.211	1.474
Fe1				0.630 <sup>*2</sup>				0.468 <sup>*2</sup>	0.409 <sup>*2</sup>		0.113	0.211	3.013
Fe2			0.536 <sup>*2</sup>					0.507 <sup>*2</sup>	0.431 <sup>*2</sup>				2.949
Fe3	0.481				0.481	0.550	0.647		0.521	0.304			2.984
P1	1.300	1.231	1.105	0.940									4.576
P2					1.613	1.372	1.335	1.105					5.426
HOH									0.800				0.800
HW1		0.260								0.740			1.000
HW1'		0.190								0.810			1.000
HW2			0.180								0.820		1.000
HW2'				0.200							0.800		1.000
HW3	0.170											0.830	1.000
HW3'			0.100									0.900	1.000
$\Sigma_v$	1.950	1.916	1.921	1.770	2.385	2.013	1.983	2.081	2.162	1.961	1.949	2.151	

Notes: Bond strengths from Brese and O'Keeffe (1991); hydrogen-bond strengths from Brown and Altermatt (1985) based on O-O bond distances; valence summations are expressed in valence units. For the bond-valence calculations, the Na/Ca site is assumed to be equally occupied by Na and Ca.

bearthite, vauquelinite, mélonjosephite, and the minerals of the brackebuschite group (Humnicki and Hawthorne 2002). The second chain is a novel double-strand arrangement in which each strand is made up of alternating corner-sharing octahedra and tetrahedra (Fig. 4b). The two strands are “out of phase” in the sense that octahedra in one strand align with and link to tetrahedra in the other strand.

Although mélonjosephite,  $\text{Ca}_2(\text{Fe}_{0.5}^{2+}\text{Fe}_{0.5}^{3+})_4(\text{PO}_4)_4(\text{OH})_2$ , has an octahedral-tetrahedral framework structure (Kampf and Moore 1977), the framework is condensed from structural layers in which linkages of octahedra and tetrahedra bear striking similarities to those in the structure of kapundaite. In mélonjosephite, the *trans*-edge-sharing chains mentioned above also occur, and are cross-linked into a sheet by a second type of octahedral-tetrahedral chain. The second chain is also a double strand, and each strand is made up of alternating corner-sharing octahedra and tetrahedra as in kapundaite. However, in mélonjosephite, adjacent strands are displaced by  $c/2$  (corresponding to  $a/2$  of kapundaite) and thus are “in phase;” they are linked together not by corner-sharing of  $\text{PO}_4$  and  $\text{Fe}(\text{O},\text{OH})_6$  groups but via sharing

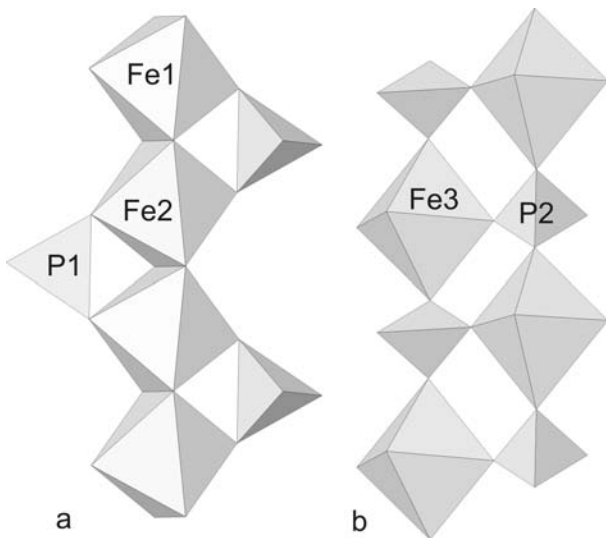


**FIGURE 4.** Two types of chains in kapundaite with the **a** axis vertical: (a) edge-sharing octahedral chain decorated with tetrahedra and (b) corner-sharing, “out-of-phase,” double-strand chain of octahedra and tetrahedra.

of octahedral edges to form octahedral dimers. The linkages of octahedra and tetrahedra in the sheet portions of the two structures are compared in Figure 5. In this figure, the tetrahedra decorating the edge-sharing chains in each structure have been omitted for clarity.

Comparing the octahedral and tetrahedral linkage topo-

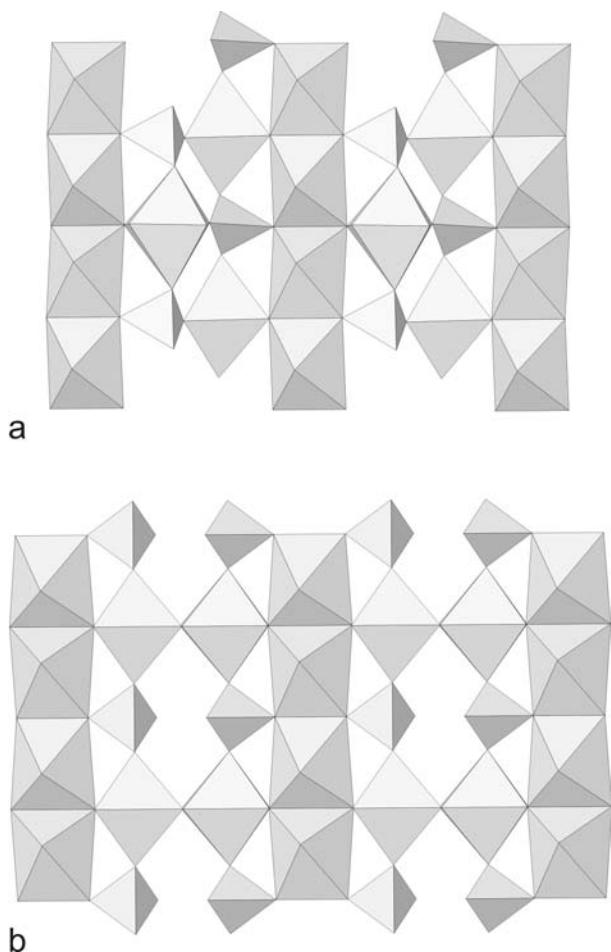


**FIGURE 5.** Linkages between edge-sharing octahedral chains in kapundaite (a) and mélonjosephite (b).

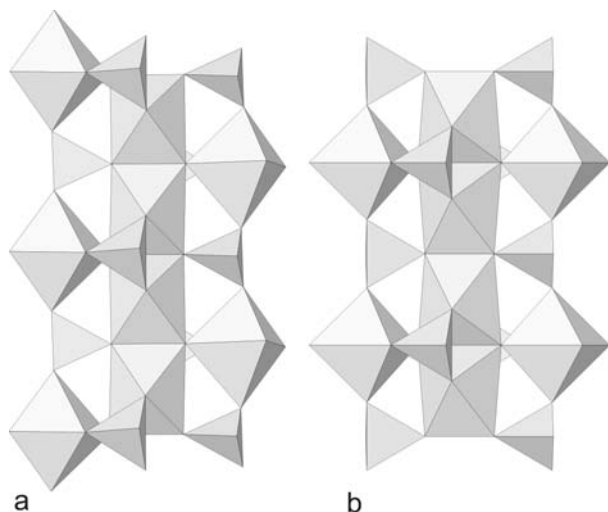


FIGURE 6. Complete octahedral-tetrahedral linkages surrounding edge-sharing octahedral chains in kapundaite (a) and mélonjosephite (b).

gies surrounding the edge-sharing octahedral chains in the two structures (Fig. 6), it is seen that the only difference is a similar “phase shift” of the  $\text{PO}_4\text{-Fe}(\text{O},\text{OH})_6$  strands on either side of the edge-sharing chains. In kapundaite, the strands are “out of phase” such that one side of the shared octahedral edge connects to an octahedron in one strand, while the other end connects to a tetrahedron in the strand on the opposite side. In mélonjosephite, the “in phase” arrangement results in both ends of the shared octahedral edges being connected to either octahedra or tetrahedra.

The kapundaite and mélonjosephite layers have the same stoichiometry, and can be regarded as different stackings of topologically identical rod-like structure modules, each of which is half of an edge-sharing octahedral chain plus the associated  $\text{PO}_4\text{-Fe}(\text{O},\text{OH})_6$  strand. The layer topologies can be converted into each other by displacement of every other such unit by half a lattice vector parallel to its length. The different inter-strand connection patterns cause the layer of kapundaite to be much more corrugated than that of mélonjosephite, resulting in a smaller unit mesh for the layer ( $6.374 \times 7.698 \text{ \AA}$  as opposed to  $6.317 \times 9.542 \text{ \AA}$ ). The layers of mélonjosephite are polymerized into a framework, since the bridging O atoms between  $\text{Fe}_2\text{X}_{10}$  dimers of one layer belong to the  $\text{PO}_4$  groups decorating the edge-sharing  $\text{Fe}_2\text{X}_8$  chains of the adjacent layers (Fig. 7), but no such linkage occurs in kapundaite, which contributes to the greater proportion of non-phosphate anions in the overall formula, along with the extra water molecules in the interlayer space.

An interesting result of the different linkage arrangements in kapundaite is that the shared octahedral edges in the chain are all equivalent, while in mélonjosephite there are two different types of shared octahedral edges. Mélonjosephite has equal proportions of  $\text{Fe}^{2+}$  and  $\text{Fe}^{3+}$ , unlike kapundaite, but there is no significant difference in mean Fe-O distances for Fe1 and Fe2, implying long-range disorder of the two oxidation states. The asymmetric coordination of the Fe atoms in the edge-sharing chain in mélonjosephite leads to alternating Fe-Fe distances of 2.97 and

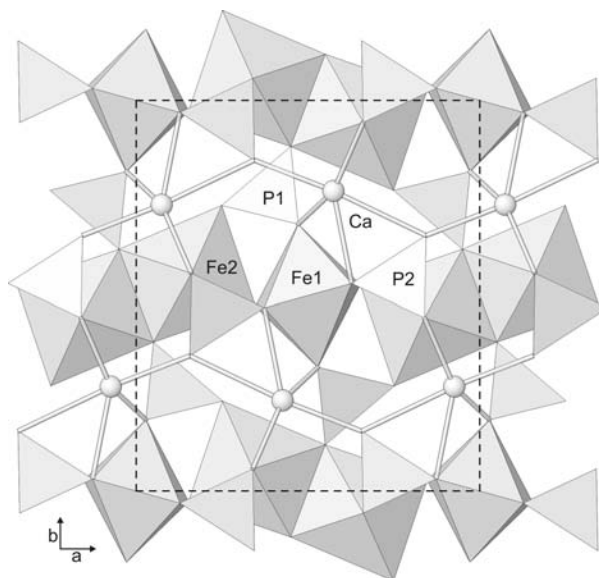


FIGURE 7. Structure of mélonjosephite viewed down c. Unit-cell outline in dashes.

$3.40 \text{ \AA}$  along the chain, a Peierls-like distortion that may imply local pairing of  $2+$  and  $3+$  cations. As seen in Figures 5b and 6b, the long shared octahedral edge ( $2.97 \text{ \AA}$ ) corresponds to the short Fe-Fe distance (which would tend to destabilize adjacent  $\text{Fe}^{3+}\cdots\text{Fe}^{3+}$  but favor  $\text{Fe}^{2+}\cdots\text{Fe}^{2+}$ ) and the short octahedral edge ( $2.51 \text{ \AA}$ ) corresponds to the long Fe-Fe distance. Presumably, electron hopping prevents long-range order being attained at room temperature. In contrast, the Fe-Fe distances along the edge-sharing chain in kapundaite are all  $3.16 \text{ \AA}$ .

#### ACKNOWLEDGMENTS

Referees Frédéric Hatert and Franz Pertlik provided helpful comments on the manuscript that are greatly appreciated. NSERC Canada is thanked for a Discovery Grant to M.R. Part of this study was funded by the John Jago Trelawney Endowment to the Mineral Sciences Department of the Natural History Museum of Los Angeles County. The structure data collection was performed at ChemMatCARS, Sector 15, Advanced Photon Source at Argonne National Laboratory. ChemMatCARS Sector 15 is principally supported by the National Science Foundation/Department of Energy under grant number CHE-0535644. Use of the Advanced Photon Source was supported by the U.S. Department of Energy, Office of Science, Office of Basic Energy Sciences, under contract no. DE-AC02-06CH11357.

#### REFERENCES CITED

- Birch, W.D., Pring, A., Self, P.G., Gibbs, R.B., Keck, E., Jensen, M.C., and Foord, E.E. (1996) Meurigite, a new fibrous iron phosphate resembling kidwellite. *Mineralogical Magazine*, 60, 787–793.
- Breese, N.E. and O’Keeffe, M. (1991) Bond-valence parameters for solids. *Acta Crystallographica*, B47, 192–197.
- Brown, I.D. and Altermatt, D. (1985) Bond-valence parameters from a systematic analysis of the inorganic crystal structure database. *Acta Crystallographica*, B41, 244–247.
- Bruker (2003) SAINT, SADABS and SHELXTL. Bruker AXS Inc., Madison, Wisconsin.
- Drexel, J.F. and Preiss, W.V. (1995) The geology of South Australia, vol. 2, The Phanerozoic. Geological Survey of South Australia Bulletin 54.
- Harrowfield, J.R., Segnit, E.R., and Watts, J.A. (1981) Aldermanite, a new magnesium aluminium phosphate. *Mineralogical Magazine*, 44, 59–62.
- Huminicki, D.M.C. and Hawthorne, F.C. (2002) The crystal chemistry of the phosphate minerals. In M.L. Kohn, J. Rakovan, and J.M. Hughes, Eds., *Phosphates—Geochemical, Geobiological, and Materials Importance*, 48, p. 123–253. *Reviews in Mineralogy and Geochemistry*, Mineralogical Society of America, Chantilly, Virginia.

- Jack, R.L. (1919) The phosphate deposits of South Australia. Geological Survey of South Australia Bulletin 7.
- Johns, R.K. (1962) South Australian rock phosphate deposits. Mining Review Adelaide, 114, 22–30.
- Kampf, A.R. and Moore, P.B. (1977) Melonjosephite, calcium iron hydroxy phosphate: its crystal structure. *American Mineralogist*, 62, 60–66.
- Kampf, A.R., Pluth, J.J., and Chen, Y.-S. (2007) The crystal structure of meurigite. *American Mineralogist*, 92, 1518–1524.
- Kampf, A.R., Adams, P.M., Kolitsch, U., and Steele, I.M. (2009) Meurigite-Na, a new species, and the relationship between phosphofibrite and meurigite. *American Mineralogist*, 94, 720–727.
- Laugier, J. and Bochu, B. (2004) Chekcell: Graphical powder indexing cell and space group assignment software, <http://www.ccp14.ac.uk/tutorial/lmgp/>.
- Mandarino, J.A. (1981) The Gladstone-Dale relationship. IV. The compatibility concept and its application. *Canadian Mineralogist*, 19, 441–450.
- Mills, S.J. (2003) A note on perhamite from the Moculta (Klemms) phosphate quarry, South Australia. *Australian Journal of Mineralogy*, 9, 43–45.
- Mills, S., Grey, I., Mumme, G., and Bordet, P. (2006) The crystal structure of perhamite. *Mineralogical Magazine*, 70, 201–209.
- Mills, S.J., Groat, L.A., Wilson, S.A., Birch, W.D., Whitfield, P.S., and Raudsepp, M. (2008) Angastonite,  $\text{CaMgAl}_2(\text{PO}_4)_2(\text{OH}) \cdot 7\text{H}_2\text{O}$ , a new phosphate mineral from Angaston, South Australia. *Mineralogical Magazine*, 72, 1011–1020.
- Pilkington, E.S., Segnit, E.R., and Watts, J.A. (1982) Peisleyite, a new sodium aluminum sulfate phosphate. *Mineralogical Magazine*, 46, 449–452.
- Segnit, E.R. and Watts, J.A. (1981) Mineralogy of the rock phosphate deposit at Moculta, South Australia. *Australian Mineralogist*, 35, 179–186.
- Sheldrick, G.M. (2008) A short history of SHELX. *Acta Crystallographica*, A64, 112–122.

MANUSCRIPT RECEIVED NOVEMBER 26, 2009

MANUSCRIPT ACCEPTED JANUARY 26, 2010

MANUSCRIPT HANDLED BY G. DIEGO GATTA